Supporting Information

Over-stoichiometry in Heavy Metal Oxides: The Case of Iono-Covalent Tantalum Trioxides

Yun-jae Lee, Taehun Lee, and Aloysius Soon*

Department of Materials Science and Engineering, Yonsei University, Seoul 03722, S. Korea

E-mail: aloysius.soon@yonsei.ac.kr

Phone: +82-2-2123-5839

Structure and energetics

Using the VASP code, we have tested various *xc* functionals to decide which one provides the most accurate (or balanced) description of the structural parameters for TaO_3. The GGA-PBE, PBEsol and self-consistent nonlocal van der Waals force (vdW)-corrected optB88 *xc* are used to perform the structural optimization for different structural configurations of TaO_3 structures. In the comparison of an optimized vertical distance between the levels of upper and bottom oxygen atoms ($d_{O-O'}$) of layered structure (Figure 1(c) of the main text) with that value of experiment, PBEsol and optB88 *xc* show the most good agreement within 5.30 % difference with respect to experimental value.[1] The computed structural properties of TaO_3 with optB88 *xc* and with PBE and PBEsol *xc* are listed in Table S1.

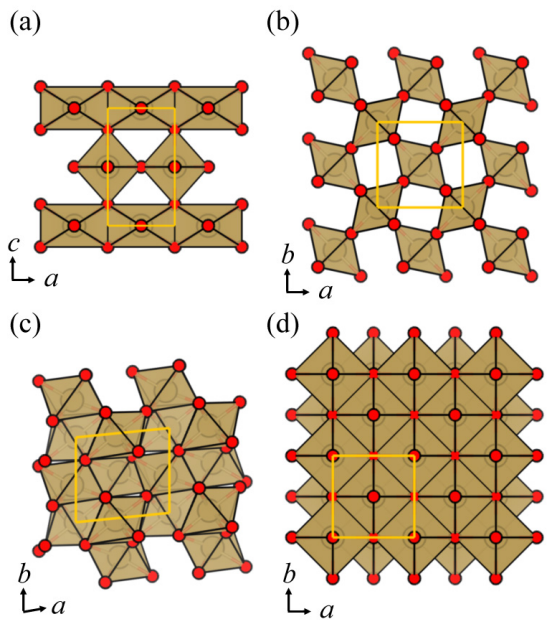

Figure S1: Crystal structures and atomic geometries of (a) β-Ta_2O_5, (b) R-TaO_2, (c) T-TaO_2, and (d) TaO. The O and Ta atoms are denoted by the red and khaki colored spheres, respectively. The connecting polyhedrons are shown in khaki and the unit cells are depicted with yellow lines.

Table S1: Lattice properties (a, b, c, and $d_{\mathrm{O-O'}}$, in Å and α, β, γ, in °), space group, and energetics (ΔH^{f}, in eV/atom) for various Ta-O compounds. Our theoretical values are calculated using the PBE, PBEsol and optB88 xc functionals as implemented in the VASP code. Other theoretical and relevant experimental values are also listed.

	Structure	a	b	c	α	β	γ	$d_{\mathrm{O-O'}}$	Space group	ΔH^{f}
PBE	α-TaO_3	3.95	3.95	3.95	90	90	90	-	$Pm3m$	−2.59
	β-TaO_3	9.80	8.92	5.37	90	98.3	90	6.94	$C2/m$	−2.63
PBEsol	α-TaO_3	3.92	3.92	3.92	90	90	90	-	$Pm3m$	−2.81
	β-TaO_3	9.70	8.81	5.28	90	97.7	90	6.92	$C2/m$	−2.87
optB88	TaO	4.50	4.50	4.50	90	90	90	-	Fm-$3m$	−1.35
	R-TaO_2	4.98	4.98	2.89	90	90	90	-	$P4_2/mnm$	−3.16
	T-TaO_2	4.69	5.20	5.72	90.1	87.2	95.7	-	P-1	−3.20
	β-Ta_2O_5	3.70	3.89	6.49	90	90	90	-	$Pmmm$	−3.10
ref.	R-TaO_2[2]	4.71	4.71	3.07	90	90	90	-	$P4_2/mnm$	-
	T-TaO_2[2]	4.70	5.20	5.72	90	87.3	95.7	-	P-1	-
	β-Ta_2O_5[3]	3.67	3.86	6.43	90	90	90	-	$Pmmm$	-
	α-TaO_3[4]	3.95	3.95	3.95	90	90	90	-	$Pm3m$	−2.77
exp.	TaO[5]	4.43	4.43	4.43	90	90	90	-	Fm-$3m$	-
	TaO_2[5]	4.71	4.71	3.07	90	90	90	-	$P4_2/mnm$	-
	β-Ta_2O_5[6]	3.68	3.90	6.22	90	90	90	-	$Pmmm$	-
	TaO_3[1]	9.60	8.43	7.33	90	94.5	90	6.62	$C2/m$	-
	$RbTaO_3$[7]	9.85	8.51	8.14	90	94.9	90	6.62	$C2/m$	-

Table S2: Lattice properties (a, b, c, and $d_{\mathrm{O-O'}}$, in Å and α, β, γ, in °), space group, and energetics (ΔH^{f}, in eV/atom) for various TaO_3 polyphases. Our theoretical values are calculated using the PBE, PBEsol and optB88 xc functionals as implemented in the Quantum-ESPRESSO package.

	Structure	a	b	c	α	β	γ	$d_{\mathrm{O-O'}}$	Space group	ΔH^{f}
PBE	α-TaO_3	3.94	3.94	3.94	90	90	90	-	$Pm3m$	−2.65
	β-TaO_3	9.77	8.96	5.27	90	97.1	90	6.94	$C2/m$	−2.68
PBEsol	α-TaO_3	3.91	3.91	3.91	90	90	90	-	$Pm3m$	−2.96
	β-TaO_3	9.66	8.80	5.26	90	98.0	90	6.92	$C2/m$	−3.01
optB88	α-TaO_3	3.92	3.92	3.92	90	90	90	-	$Pm3m$	−3.45
	β-TaO_3	9.73	8.84	5.34	90	99.1	90	6.92	$C2/m$	−3.49

For cross-checking, DFT calculations using periodic supercell model are also performed with the Quantum-ESPRESSO package.[8] Here, ultrasoft pseudopotentials were used with the plane wave kinetic energy cutoff of 50 Ry.[9] A Γ-centered **k**-point mesh with a spacing of 0.2 $\mathrm{Å}^{-1}$ is used to sample the Brillouin-zone, which is same as our detail with VASP code (as detailed in the main text). For the energetics of various tantalum oxide structures, we have tested a few semi-local approximations to the xc functional – namely that due to Perdew, Burke, and Ernzerhof (PBE)[10] and its revised form for solids (PBEsol),[11] as well as the self-consistent van der Waals (vdW) corrected xc functional, optB88.[12,13]

Elastic and dynamical stability

Table S3: Calculated elastic constants C_{ij} (in GPa) for α-TaO_3, β-TaO_3 and β'-TaO_3 using the optB88 xc functional. Other theoretical values[4] are included for comparison.

	α-TaO_3	β-TaO_3	β'-TaO_3	α-TaO_3 [4]
C_{11}	480.1	162.1	18.5	487.6
C_{22}	-	115.2	19.3	-
C_{33}	-	133.8	-	-
C_{44}	35.6	11.3	6.4	34.6
C_{55}	-	42.6	-	-
C_{66}	-	20.8	-	-
C_{12}	47.3	43.5	4.9	52.7
C_{13}	-	70.0	-	-
C_{23}	-	52.2	-	-
C_{15}	-	-23.1	-	-
C_{25}	-	-3.8	-	-
C_{35}	-	-47.8	-	-
C_{46}	-	1.4	-	-

For α-TaO_3 or cubic system, the stability criteria is as follow,

$$C_{11} + 2C_{12} > 0, C_{44} > 0, C_{11} - C_{12} > 0 \tag{1}$$

For β-TaO_3 or monoclinic system,

$$C_{11}, C_{22}, C_{33}, C_{44}, C_{55}, C_{66} > 0, \tag{2}$$

$$[C_{11} + C_{22} + C_{33} + 2(C_{12} + C_{13} + C_{23})] > 0,$$

$$(C_{33}C_{55} - C_{35}^2) > 0, (C_{44}C_{66} - C_{46}^2) > 0,$$

$$(C_{22} + C_{33} - 2C_{23}) > 0,$$

$$[C_{22}(C_{33}C_{55} - C_{35}^2) + 2C_{23}C_{25}C_{35} - C_{23}^2C_{55} - C_{25}^2C_{33}] > 0,$$

$$2[C_{15}C_{25}(C_{33}C_{12} - C_{13}C_{23}) + C_{15}C_{35}(C_{22}C_{13} - C_{12}C_{23}) + C_{25}C_{35}(C_{11}C_{23} - C_{12}C_{13})]$$

$$-[C_{15}^2(C_{22}C_{33} - C_{23}^2) + C_{25}^2(C_{11}C_{33} - C_{13}^2) + C_{35}^2(C_{11}C_{22} - C_{12}^2)] + gC_{55} > 0$$

$$(g = C_{11}C_{22}C_{33} - C_{11}C_{23}^2 - C_{22}C_{13}^2 - C_{33}C_{12}^2 + 2C_{12}C_{13}C_{23})$$

For β'-TaO_3 or 2D system,

$$C_{11}C_{22} - C_{12}^2 > 0, C_{11}, C_{22}, C_{44} > 0 \tag{3}$$

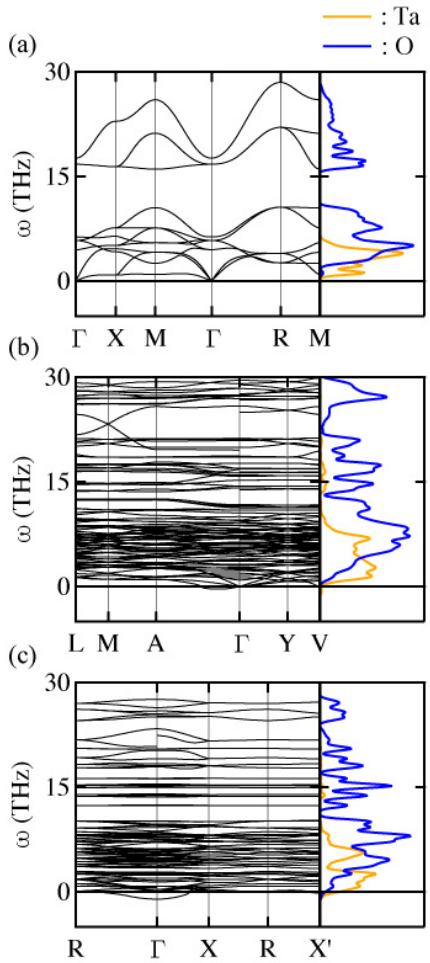

Figure S2: Phonon dispersion plots (as shown on the left panel) with the corresponding projected phonon density-of-states (as shown on the right panel) for (a) α-TaO_3, (b) β-TaO_3, and (c) β'-TaO_3. These are calculated using the optB88 xc functional as implemented in the VASP code.

For cross-checking, density functional perturbation theory (DFPT) calculations using periodic supercell model with the Quantum-ESPRESSO package[8] are also performed. For the lattice dynamics with β-TaO_3, phonon frequencies are calculated within the DFPT framework. $2 \times 2 \times 3$ **q**-point grids are used for the β-TaO_3. We also consider the LO-TO splitting in our final phonon dispersion plot as shown in Figure S3.

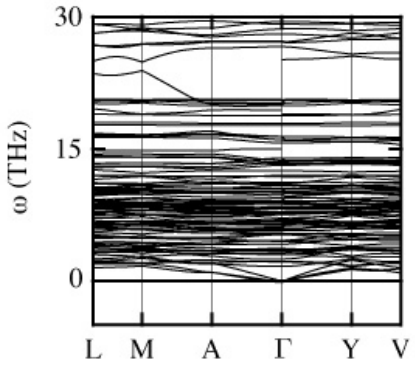

Figure S3: Phonon dispersion plot of β-TaO_3 calculated using the optB88 xc functional as implemented in the Quantum-ESPRESSO package.

Chemical bonding analysis

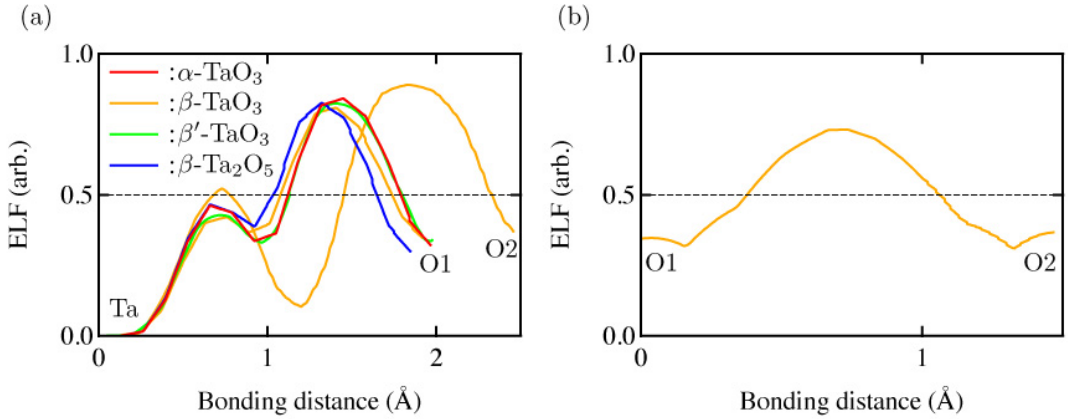

Figure S4: Electron localization function (ELF) line profiles for α-TaO_3 (red line), β-TaO_3 (yellow line) to 2 different oxygen (namely O1 and O2 in Fig. 4), β'-TaO_3 (green line) and β-Ta_2O_5 (blue line), and (b) between O1 and O2 for β-TaO_3. Dotted horizontal line located at the 0.5 of ELF value indicates the covalent nature.

Optical responses

Using the independent-particle approximation (IPA) approach,[14] we calculate the optical responses for the polymorphs of TaO_3 studied in this work. Despite of neglecting the excitonic and local-field effects, the IPA approach seems rather successful in providing a qualitative picture of the dielectric properties of many metal oxides.[15–17]

Briefly, for the interband transitions, the imaginary part of the dielectric function, $\epsilon_2^{\alpha\beta}(\omega)$ is obtained upon the summation over the empty states as follows,

$$\epsilon_2^{\alpha\beta}(\omega) = \frac{4\pi^2 e^2}{\Omega} \lim_{q\to 0} \frac{1}{q^2} \sum_{c,v,\mathbf{k}} 2\omega_{\mathbf{k}} \delta(\epsilon_{c\mathbf{k}} - \epsilon_{v\mathbf{k}} - \omega) \times \langle u_{c\mathbf{k}+\mathbf{e}_\alpha q} | u_{v\mathbf{k}} \rangle \langle u_{c\mathbf{k}+\mathbf{e}_\beta q} | u_{v\mathbf{k}} \rangle^* \quad , \qquad (4)$$

where Ω, q, c, v, α, and β are the volume of the unit cell, the Blöch vector of incident wave, the states in the conduction bands, the states in the valence bands, and two Cartesian factors, respectively. Also, the periodic part of the Kohn-Sham orbitals ($\psi_i^{\mathbf{k}}(\mathbf{r})$) at the $\mathbf{k}$-point, $\mathbf{k}$ is represented as $u_{c\mathbf{k}} = e^{-i\mathbf{k}\cdot\mathbf{r}} \psi_i^{\mathbf{k}}(\mathbf{r})$. The real part of dielectric function, $\epsilon_1^{\alpha\beta}(\omega)$ is

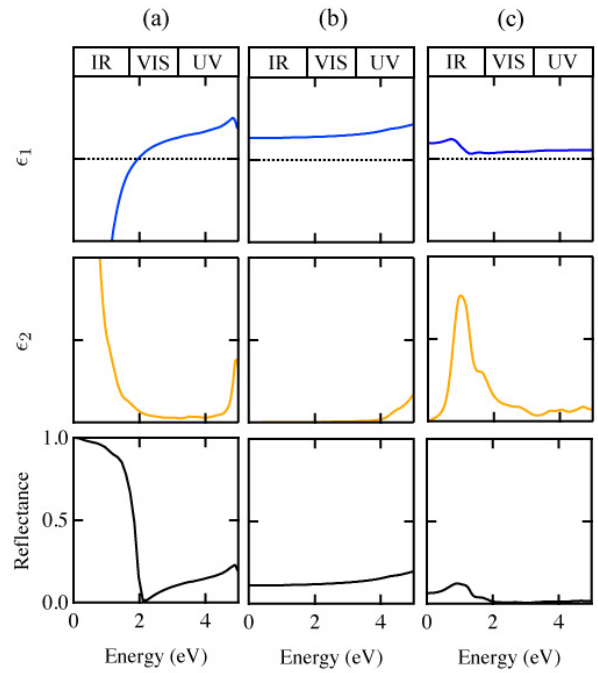

Figure S5: HSE06 computed the real and imaginary part of the dielectric function (ϵ_1, ϵ_2) with Drude-like corrections and the reflectance (R) with IPA for (a) α-TaO_3, (b) β-TaO_3 and (c) β'-TaO_3.

then derived via the Kramers-Kronig transformation, yielding

$$\epsilon_1^{\alpha\beta}(\omega) = 1 + \frac{2}{\pi}\mathrm{P}\int_0^\infty \frac{\epsilon_2^{\alpha\beta}(\omega')\omega'}{\omega'^2 - \omega^2} d\omega' \quad . \tag{5}$$

For the metallic intraband transitions, we add a Drude-like correction term to both the imaginary and real parts of dielectric functions, following Reference 18,

$$\epsilon_2^{\mathrm{Drude}}(\omega) = \frac{\Gamma\omega^2}{\omega(\omega^2 + \Gamma^2)} \quad , \tag{6}$$

and

$$\epsilon_1^{\mathrm{Drude}}(\omega) = 1 - \frac{\omega^2}{\omega(\omega^2 + \Gamma^2)} \quad , \tag{7}$$

where Γ is taken as the lifetime broadening in the Drude model. Here, we adopt a lifetime broadening value of 0.1 eV which is commonly used for most elemental metals.[19]

From the Drude-corrected total dielectric function, we compute and obtain the refractive

index (n), the extinction coefficient (k) and finally, the reflectance (R) from,

$$n = \frac{\sqrt{\epsilon_1 + \sqrt{\epsilon_1^2 + \epsilon_2^2}}}{\sqrt{2}} \quad , \tag{8}$$

$$k = \frac{\sqrt{-\epsilon_1 + \sqrt{\epsilon_1^2 + \epsilon_2^2}}}{\sqrt{2}} \quad , \tag{9}$$

and

$$R = \frac{(n-1)^2 + k^2}{(n+1)^2 + k^2} \quad . \tag{10}$$

References

(1) Fukuda, K.; Nakai, I.; Ebina, Y.; Ma, R.; Sasaki, T. Colloidal Unilamellar Layers of Tantalum Oxide with Open Channels. *Inorg. Chem.* **2007**, *46*, 478.

(2) Zhu, L.; Zhou, J.; Guo, Z.; Sun, Z. Realization of a Reversible Switching in TaO_2 Polymorphs via Peierls Distortion for Resistance Random Access Memory. *Appl. Phys. Lett.* **2015**, *106*, 091903.

(3) Cui, Z. H.; Jiang, H. Theoretical Investigation of Ta_2O_5, TaON, and Ta_3N_5: Electronic Band Structures and Absolute Band Edges. *J. Phys. Chem. C* **2017**, *121*, 3241–3251.

(4) Ravi, C.; Kaur, G.; Bharathi, A. First-principles Study of Lattice Stability of ReO_3-type Hypothetical TaO_3. *Comput. Mat. Sci.* **2014**, *90*, 177.

(5) Schönberg, N. An X-Ray Investigation of the Tantalum-Oxygen System. *Acta Chem. Scand.* **1954**, *8*, 240–245.

(6) Aleshina, L. A.; Loginova, S. V. Rietveld Analysis of X-ray Diffraction Pattern from β-Ta_2O_5 Oxide. *Crystallogr. Rep.* **2002**, *47*, 415–419.

(7) Serafin, M.; Hopper, R. Coordination Number 5 and 6 in $RbTaO_3$: $Rb_4{}^2[Ta_4O_{12}]$. *Angew. Chem.* **1978**, *90*, 387–387.

(8) Giannozzi, P.; Baroni, S.; Bonini, N.; Calandra, M.; Car, R.; Cavazzoni, C.; Ceresoli, D.; Chiarotti, G. L.; Cococcioni, M.; Dabo, I. et al. QUANTUM ESPRESSO: a Modular and Open-source Software Project for Quantum Simulations of Materials. *J. Phys. Condens. Matter* **2009**, *21*, 395502.

(9) Vanderbilt, D. Soft Self-consistent Pseudopotentials in a Generalized Eigenvalue Formalism. *Phys. Rev. B* **1990**, *41*, 7892–7895.

(10) Perdew, J. P.; Burke, K.; Ernzerhof, M. Generalized Gradient Approximation Made Simple. *Phys. Rev. Lett.* **1996**, *77*, 3865.

(11) Perdew, J. P.; Ruzsinszky, A.; Csonka, G. I.; Vydrov, O. A.; Scuseria, G. E.; Constantin, L. A.; Zhou, X.; Burke, K. Restoring the Density-gradient Expansion for Exchange in Solids and Surfaces. *Phys. Rev. Lett.* **2008**, *100*, 136406.

(12) Klimeš, J.; Bowler, D. R.; Michaelides, A. Chemical Accuracy For the Van Der Waals Density Functional. *J. Phys.: Condens. Matter* **2010**, *22*, 022201.

(13) Klimeš, J.; Bowler, D. R.; Michaelides, A. Van der Waals Density Functionals Applied to Solids. *Phys. Rev. B* **2011**, *83*, 195131.

(14) Gajdos, M.; Hummer, K.; Kresse, G.; Furthmüller, J.; Bechstedt, F. Linear Optical Properties in the Projector-augmented Wave Methodology. *Phys. Rev. B* **2006**, *73*, 045112.

(15) Gavrilenko, V. I.; Bechstedt, F. Local-field and exchange-correlation effects in optical spectra of semiconductors. *Phys. Rev. B* **1996**, *54*, 13416–13419.

(16) Walsh, A.; Yan, Y.; Huda, M. N.; Al-Jassim, M. M.; Wei, S.-H. Band Edge Electronic

Structure of $BiVO_4$: Elucidating the Role of the Bi s and V *d* Orbitals. *Chem. Mater.* **2009**, *21*, 547–551.

(17) Lee, Y.; Lee, T.; Jang, W.; Soon, A. Unraveling The Intercalation Chemistry Of Hexagonal Tungsten Bronze And Its Optical Responses. *Chem. Mater.* **2016**, *28*, 4528–4535.

(18) Lashgari, H.; Abolhassani, M. R.; Boochani, A.; Elahi, S. M.; Khodadadi, J. Electronic and Optical Properties of 2D Graphene-like Compounds Titanium Carbides and Nitrides: DFT Calculations. *Solid State Commun.* **2014**, *195*, 61–69.

(19) Werner, W. S. M.; Glantschnig, K.; Ambrosch-Draxl, C. Optical Constants and Inelastic Electron-Scattering Data for 17 Elemental Metals. *J. Phys. Chem. Ref. Data* **2009**, *38*, 1013–1092.